Research Square

Preprints are preliminary reports that have not undergone peer review.
They should not be considered conclusive, used to inform clinical practice,
or referenced by the media as validated information.

# A role for ABCG2 in synergistic interactions between targeted therapies

**Rene Bernards**

r.bernards@nki.nl

Netherlands Cancer Institute https://orcid.org/0000-0001-8677-3423

**João M. Fernandes Neto**

Netherlands Cancer Institute https://orcid.org/0000-0002-0549-8835

**Chrysa Papagianni**

The Netherlands Cancer Institute

**Niki Pouliopoulou**

The Netherlands Cancer Institute

**Cor Lieftink**

Netherlands Cancer Institute https://orcid.org/0000-0002-2754-4150

**Ben Morris**

Netherlands Cancer Institute

**Ernest Nadal**

Catalan Institute of Oncology, Bellvitge Biomedical Research Institute (IDIBELL)
https://orcid.org/0000-0002-9674-5554

**Enriqueta Felip**

Vall d'Hebron Institute of Oncology, Vall d'Hebron Barcelona Hospital Campus

**Lourdes Farre**

Program Against Cancer Therapeutic Resistance (ProCURE), Catalan Institute of Oncology (ICO),
https://orcid.org/0000-0002-3168-1940

**Juan Francisco Martin Tejera**

Catalan Institute of Oncology (ICO)

**August Vidal**

Bellvitge University Hospital https://orcid.org/0000-0001-5727-2099

**Alberto Villanueva**

Institut Català d'Oncologia (ICO)-Institut d'Investigació Biomèdica de Bellvitge (IDIBELL)
https://orcid.org/0000-0001-5164-0006

**Roderick Beijersbergen**

Netherlands Cancer Institute https://orcid.org/0000-0003-0116-4130

**Matheus Dias**

Netherlands Cancer Institute

**Article**

**Keywords:**

**Posted Date:** June 1st, 2026

**DOI:** https://doi.org/10.21203/rs.3.rs-9858448/v1

**License:** This work is licensed under a Creative Commons Attribution 4.0 International License.
Read Full License

**Additional Declarations: Yes** there is potential Competing Interest. Alberto Villanueva and August Vidal: • co-founders and shareholders of Xenopat S.L. (Barcelona, Spain). Ernest Nadal: • Research funding: Roche, Pfizer, Merck-Serono, Bristol Myers Squibb and Boehringer-Ingelheim. • Advisory board or lectures: Amgen, Apollomics, AstraZeneca, BeiGene, BMS, Boehringer-Ingelheim, Daiichi-Sankyo, Genmab, Glaxo Smith Kline, Illumina, Johnson & Johnson, Lilly, Merck Sharp & Dohme (MSD), Merck-Serono, Pfizer, PharmaMar, Pierre Fabre, Qiagen, Regeneron, Roche, Sanofi, Summit Therapeutics and Takeda. • Travel support: Roche, Takeda, Janssen and MSD.

# Abstract

Despite advances in targeted anti-cancer therapy in EGFR-mutant Non-Small Cell Lung Cancer (NSCLC), resistance is still almost inevitable. Identifying combination strategies that can treat drug-resistant tumors effectively is an urgent clinical need. Importantly, accurate mechanistic understanding of these combinations is essential for their optimal clinical development. Here, we aimed to identify stress-related vulnerabilities associated with resistance to EGFR inhibition in NSCLC cells. Using a stress-focused compound library, we screened gefitinib-resistant PC9 cells and identified barasertib, an Aurora kinase B inhibitor, as a vulnerability of drug-resistant cells. Surprisingly, this vulnerability was strictly dependent on the presence of EGFR inhibitor gefitinib, but independent of EGFR signaling inhibition. Mechanistic investigation, including a genome-wide CRISPR screen, revealed that the synergistic interaction between gefitinib and barasertib is mediated by ABCG2 (ATP Binding Cassette Subfamily G Member 2), a critical drug efflux pump. Our data indicate that gefitinib reduces barasertib efflux, thereby increasing its intracellular accumulation and target engagement at lower, non-toxic concentrations. This combination strategy was validated in multiple EGFR inhibitor-resistant models in vitro and in vivo using patient-derived xenograft models. Furthermore, we demonstrate that this concept is generalizable. By performing a large-scale drug repurposing screen, we identified multiple clinically approved drugs with diverse targets that act as ABCG2 inhibitors and sensitize cancer cells to barasertib. We conclude that the ability of a drug to act as an ABC transporter inhibitor – beyond its original target inhibition – represents an underappreciated mechanism with potential for increasing the efficacy of targeted anti-cancer agents. This approach provides a rational, highly translatable paradigm for designing drug combinations that can reduce effective dosage and thereby potentially revive drugs previously discontinued due to toxicity.


# Introduction

Lung cancer is one of the most frequently diagnosed cancer types worldwide. Recent progress in early detection through screening has advanced its clinical management and has changed the course of the disease for some patients. Nevertheless, lung cancer remains the leading cause of cancer-related deaths globally[1]. Poor response to conventional chemotherapy and radiotherapy is a hallmark of these tumors[2]. Among histological subtypes, non-small cell lung cancer (NSCLC) is by far the most common, accounting for approximately 85 percent of all lung cancer cases[3]. About 30 percent of advanced NSCLC tumors harbor gain-of-function mutations in the epidermal growth factor receptor (*EGFR*)[4], which led to the development and clinical implementation of multiple EGFR inhibitors. Unfortunately, despite substantial initial responses, EGFR-driven tumors almost invariably resume progression under continued drug exposure. Some of the mechanisms of acquired resistance are well understood[5,6], such as a secondary T790M mutation in *EGFR* which often emerged during treatment with first generation anti-EGFR inhibitors. The current first-line treatment landscape consists of using third- generation EGFR inhibitors alone or combined with platinum-based chemotherapy or with a bispecific monoclonal

antibody targeting EGFR and MET[7,8]. However, resistance to these inhibitors also emerges, limiting improvements in overall survival[6,9].

Aurora kinases have previously been proposed as therapeutic targets to prevent or overcome resistance to EGFR inhibition in NSCLC models. For example, Tanaka and colleagues reported that combined inhibition of EGFR and Aurora kinase B induces apoptosis mediated by BIM and PUMA in osimertinib-sensitive models, and that cells with acquired resistance to EGFR inhibitors become hypersensitive to Aurora B inhibition[10]. Independently, Shah and colleagues showed that Aurora kinase A activity supports persistence and resistance to third-generation EGFR inhibitors. Their work demonstrated that inhibition of both EGFR and Aurora kinase A was necessary to suppress downstream signaling and trigger a pro-apoptotic program[11].

Using both drug screens and genome-scale CRISPR screens, we identify here a critical role for the ABCG2 (ATP Binding Cassette Subfamily G Member 2) transporter in this vulnerability of gefitinib-resistant cells to the Aurora kinase B inhibitor barasertib. ABCG2 and other ABC transporters have been previously investigated as potential targets for anticancer therapies but none of the dedicated inhibitors developed have reached clinical use. Our data invite to revisit the potential of targeting ABC transporters to deepen therapeutic responses and indicate that drugs already clinically available can be exploited for this purpose.

# Results

### Gefitinib enhances the sensitivity of gefitinib-resistant PC9 cells to barasertib

Non-small cell lung cancer PC9 cells carry the exon 19 deletion mutation (E746_A750del) in EGFR, a common activating mutation that confers sensitivity to EGFR tyrosine kinase inhibitors (TKIs)[12]. To generate EGFR inhibitor-resistant models, we cultured PC9 cells for two months in the presence of 2 micromolar gefitinib, allowing multiple resistant subpopulations to emerge. We subjected these subpopulations to DNA sequencing to assess the presence of the well-known secondary T790M mutation in EGFR. We selected the GRI (T790M-negative) and GRIII (T790M-positive) subclones for subsequent studies. Treatment with 2 micromolar gefitinib abolished cell proliferation in parental PC9 cells but had no effect on GRI or GRIII cells. Both resistant sublines tolerated up to 8 micromolar gefitinib, while the IC50 in parental PC9 cells was 26 nanomolar (Figure 1A, 1B and Supplementary Figure 1A, 1B, 1C).

To identify stress-related vulnerabilities associated with EGFR inhibitor resistance, we screened a “stress-focused” library of 44 compounds (Supplementary Table 1). These compounds were selected for their ability to target different stress pathways that are commonly upregulated in cancer cells, including proteotoxic stress, DNA damage, oxidative stress, mitotic stress, metabolic stress, and evasion of apoptosis[13]. We assessed the sensitivity of GRI and GRIII cells to these compounds in the presence of 2 micromolar gefitinib, using parental PC9 cells as a control (Figure 1C). The aurora kinase B inhibitor

barasertib was the top hit of this screen (Figure 1D and Supplementary Table 2). Independent dose-response curves and long-term viability experiments confirmed the screen results and demonstrated that the presence of gefitinib is required for the increased sensitivity of GRI and GRIII cells to barasertib (Figure 1E, 1F and Supplementary Figure 1D). This data suggested a synergistic interaction between gefitinib and barasertib, rather than a collateral sensitivity acquired during resistance development. Corroborating this notion, gefitinib and barasertib are highly synergistic as judged by ZIP synergy analyses[14] in GRI and GRIII cells (Figure 1G and Supplementary Figure 1E).

In our models, gefitinib-resistant cells were not particularly sensitive to barasertib alone compared to parental PC9s (Figure 1F). We therefore assessed whether modulation of downstream EGFR signaling could explain the synergy between gefitinib and barasertib. In parental PC9 cells, gefitinib caused the expected suppression of EGFR signaling and its downstream targets. In contrast, although we observed differences in EGFR phosphorylation between GRI and GRIII cells, treatment with gefitinib, barasertib, or their combination had no discernible effect on the levels of phosphorylated ERK in either resistant line (Figure 1H). These results suggest that the synergy between gefitinib and barasertib in resistant cells does not rely on suppression of canonical EGFR downstream signaling.

**The synergy between Gefitinib and Barasertib is independent of EGFR inhibition**

We next tested whether the gefitinib-barasertib synergy could be extended to NSCLC models that are intrinsically resistant to gefitinib. We found that gefitinib-naive H1975 cells that already carry the EGFR T790M mutation and H358 (KRAS G12C mutant) cells were non-responsive to gefitinib but were highly sensitive to the combination of gefitinib and barasertib (Figure 2A). We then asked whether the synergistic drug interaction with barasertib was specific to gefitinib or if other EGFR inhibitors could substitute for gefitinib in this combination. Interestingly, the EGFR inhibitor lapatinib also sensitized GRI and GRIII cells to barasertib but EGFR-blocking monoclonal antibody cetuximab did not (Figure 2B and Supplementary Figure 2A), which suggested that the synergistic effect might be specific to small-molecule EGFR inhibitors. In line with that notion, knock-down of EGFR did not sensitize GRI and H358 cells to barasertib, while synergy with gefitinib is still observed (Figure 2C, 2D and Supplementary Figure 2B, 2C). Taken together, these data indicated that the synergistic drug interaction with barasertib is not dependent on EGFR inhibition and suppression of downstream signaling. Instead, other mechanism(s), not previously considered, appeared to underlie the vulnerability of NSCLC cells to barasertib in the presence of EGFR TKIs.

**Gefitinib reduces ABCG2-mediated barasertib efflux**

To gain insight into the possible mechanism(s) underlying the synergy between barasertib and EGFR inhibitors in our models, we performed RNA sequencing in PC9, GRI and GRIII cells treated with gefitinib, barasertib or their combination and compared them with untreated controls (Supplementary Figure 3A). Gene set enrichment analysis (GSEA) could not reveal any clear differences in the cells treated with the gefitinib-barasertib combination that were not explainable by the effect of either gefitinib or barasertib alone. To address unbiasedly the mechanisms underlying the synergy between barasertib and EGFR

inhibitors we performed a genome-wide CRISPR screen in GRI cells (Figure 3A). The aim of this screen was to identify genes whose loss would mimic the effect of gefitinib, i.e., that would sensitize GRI cells to a non-lethal low concentration of barasertib. The screen revealed that knockout of ABCG2 increased barasertib toxicity, while having no effect in the absence of the drug. ABCG2 (ATP-binding cassette sub-family G member 2) is a translocation protein used to actively pump drugs and other compounds against their concentration gradient using the hydrolysis of ATP. In addition, several guide RNAs targeting known transcriptional regulators of ABCG2, including AHR, ARNT, and EP300 were also depleted in the screen, further supporting the involvement of this transporter in the response to barasertib (Figure 3B and Supplementary Table 3). Independent validation confirmed that knockout of ABCG2 or its regulator AHR sensitized GRI, GRIII, and H1975 cells to barasertib (Figure 3C, 3D).

Previous studies have shown that barasertib is a substrate of ABCG2[15] while gefitinib has been characterized as both a high-affinity substrate and an inhibitor of ABCG2, with the specific role often depending on its concentration and the cellular context[16–20]. Based on this knowledge, we hypothesized that gefitinib enhances the efficacy of barasertib by reducing ABCG2-mediated efflux of barasertib, thereby increasing the intracellular availability of the drug. Consistent with that notion, the ABCG2 inhibitor Ko143 and the multi-kinase inhibitor imatinib, which is described as both a substrate and inhibitor of ABCG2[21], mimicked gefitinib by sensitizing resistant cells to barasertib (Figure 3E and Supplementary Figure 3B). Furthermore, the increased sensitivity to barasertib in the presence of gefitinib correlated with enhanced on-target activity of barasertib, as indicated by reduced phosphorylation of histone H3 at serine 10, a well-characterized substrate of Aurora kinase B[22,23]. A toxic high dose of barasertib alone produced similar H3 hypo-phosphorylation and induction of apoptosis, assessed by increased cleaved PARP (Figure 3F).

We further tested whether overexpression of ABCG2 was sufficient to confer resistance to barasertib. Using CRISPRa technology, we overexpressed ABCG2 in PC9 cells, which led to a reduction in sensitivity to barasertib (Figure 3G). ABCG2 overexpression also led to a reduction in sensitivity to gefitinib whereas its knock-out sensitized PC9 cells to gefitinib, corroborating previous reports that gefitinib is a substrate of ABCG2[16–20] (Figure 3H, 3I). In a complementary approach, we subjected PC9 and H1975 cells to escalating concentrations of barasertib for over two months to generate barasertib-resistant sublines. These barasertib-resistant cells exhibited increased ABCG2 expression, but their resistance could be overcome by co-treatment with gefitinib (Supplementary Figure 3C, 3D, 3E). Together, these findings demonstrate that gefitinib sensitizes NSCLC cells to barasertib by reducing ABCG2-mediated barasertib efflux, thereby increasing intracellular accumulation and enhancing target engagement at lower concentrations.

To assess potential clinical relevance of this ABCG2-mediated synergistic interaction, we tested the combination of gefitinib and barasertib in two heavily pre-treated, EGFR inhibitor-resistant patient-derived xenograft (PDX) models. In both models, adding gefitinib to barasertib suppressed tumor growth and was well tolerated by mice (Figure 3J, 3K).

**Drugs with ABCG2 activity increase the efficacy of targeted anti-cancer drugs**

Because of the strong drug synergies with barasertib mediated by ABCG2 modulation described above, we reasoned that similar interactions between other clinically relevant compounds might be uncovered. This is of particular interest because ABCG2 expression has been shown to influence the sensitivity to a wide range of therapeutic agents. Moreover, although ABC transporter activity is recognized as a key mechanism of multidrug resistance in cancer, efforts to develop clinically useful ABC transporter inhibitors have so far been unsuccessful. In this context, repurposing clinically available drugs such as gefitinib to inhibit ABCG2 and potentially improve the efficacy of other agents offers a promising alternative.

To explore this concept further, we conducted an additional screen in GRI cells using the Oncode drug repurposing library[24]. This library comprises 5632 compounds, including FDA-approved drugs, compounds in clinical trials, in pre-clinical development and tool compounds. We treated GRI cells with a single concentration of each compound in the absence of any additional drug (control arm) and in the presence of a sub-lethal concentration of barasertib (50nM), aiming to identify compounds that increased barasertib toxicity (Figure 4A). Using a threshold of 50 percent effect size and a false discovery rate of 0.4, we identified 74 hits (Supplementary Table 4).

To validate and further characterize these interactions, we selected fifty compounds for follow-up testing. We performed dose-response curves for each compound and quantified how increasing concentrations of each compound would sensitize GRI cells to the sublethal 50nM barasertib concentration (Figure 4A). Twenty-five of those compounds increased the sensitivity to barasertib significantly (Figure 4B and Supplementary Table 5). EGFR and Pan-HER inhibitors, other tyrosine kinase inhibitors and ABC transporter inhibitors were among the compounds which increased the toxicity of barasertib the most, but we also observed increased sensitivity to compounds with unrelated targets and clinical indications. We selected five compounds (OX2 receptor antagonist JNJ-10397049, pan-TRK inhibitor GNF-5837, HER2 and EGFR inhibitor lapatinib, pan-HER inhibitor BMS-599626 and the multi-receptor tyrosine kinase (RTK) inhibitor sunitinib) to assess the role of ABCG2 in these drug interactions. Knock-out of ABCG2 did not enhance the toxicity of any of these drugs (Supplementary Figure 4A, 4B), indicating they are unlikely substrates of this transporter. In contrast, sublethal doses of all five drugs increased the sensitivity to barasertib, similarly to what is observed in ABCG2-KO cells (Figure 4C and Supplementary Figure 4C, 4D). This data supports the notion that ABCG2 activity mediates the observed synergistic drug interactions and indicate that these drugs act as ABCG2 inhibitors.

Finally, to extend our investigation beyond barasertib, we tested whether similar synergistic interactions would be observed with other clinically relevant drugs whose toxicities can be modulated by ABCG2. Increased ABCG2 expression has been shown to confer resistance to danusertib (pan-Aurora kinase and ABL kinase inhibitor) and MLN4924 (NEDD8-activating enzyme inhibitor)[25,26]. Consistently, we found that for both drugs, cell viability was decreased in the presence of gefitinib or Ko143 (Figure 4D Supplementary Figure 4E). Notably, some drugs are more dependent on ABCG2 activity than others, as

illustrated by the comparison of IC50s of barasertib, danusertib and MLN4924 in the presence or absence of ABCG2 inhibitor Ko143 (Figure 4E Supplementary Figure 4F). These findings support the notion that ABCG2 activity can mediate synergistic interactions between drugs with distinct targets and mechanisms. Moreover, our research uncovered unanticipated but potentially clinically relevant drug combinations that exploit ABCG2-mediated interactions using compounds that are already available.

# Discussion

The drug attrition rate in cancer is extremely high, with estimates suggesting that up to 95% of drugs fail to reach approval. Lack of efficacy and unmanageable toxicity are the main contributing factors to this failure[27–29]. Barasertib is one such example of a drug whose clinical development has been hampered due to toxicity, despite promising efficacy[30,31]. In this study, we show that the concentration of ABCG2-dependent anti-cancer drugs can be significantly reduced by using combinations with inhibitors, or high-affinity substrates of ABCG2 (Figure 4F). For instance, the top hit from our drug repurposing screen, JNJ-10397049, a selective orexin 2 receptor antagonist developed for its potential in treating sleep disorders like insomnia is a good example of a compound that could be pursued in future clinical studies. Albeit not FDA approved, data from animal studies[32] suggest it should have a good safety profile, thereby being a good candidate for combining with anti-cancer drugs that are ABCG2 substrates. Other examples with a strong potential for clinical testing are sunitinib, ledipasvir and elbasvir, all of which are already FDA approved for different indications.

In our mouse PDX studies, adding gefitinib to a sub-optimal (below MTD) barasertib concentration was well tolerated and suppressed tumor growth. These PDX models were derived from patients who had received multiple lines of treatment, including gefitinib itself, as well as second-generation EGFR inhibitors such as erlotinib and afatinib. In addition, these patients had also been treated with platinum compounds, gemcitabine, and immunotherapy. These data show that tumors refractory to multiple lines of therapy are still responsive this strategy. However, it remains to be addressed whether combining ABCG2 substrates like barasertib with clinically available ABCG2 inhibitors would improve efficacy without added toxicity in human trials.

Third-generation EGFR inhibitors osimertinib and lazertinib are currently the most widely used first-line treatment in EGFR mutant NSCLC[7]. Interestingly, both osimertinib and lazertinib have been shown to be substrates/inhibitors of ABCG2[33–36]. Second-line therapy for osimertinib-resistant NSCLC depends on the specific mechanism of resistance. Standard options include platinum-based chemotherapy (e.g., pemetrexed) or targeted combinations like amivantamab plus chemotherapy. Standard guidelines historically recommended platinum-based chemotherapy to be given without osimertinib. However, recent data from the COMPEL trial showed that continuing osimertinib alongside platinum-pemetrexed chemotherapy in osimertinib-refractory patients significantly improved progression-free survival compared to chemotherapy alone[37]. Like many other chemotherapy agents, pemetrexed is transported by ABCG2[38]. By putting together our findings and the fact that both osimertinib and pemetrexed interact

with ABCG2, a possible explanation for the COMPEL trial positive results could be that in osimertinib-refractory patients, osimertinib still acts as a ABCG2 inhibitor, slowing-down the efflux of pemetrexed, thereby enhancing its efficacy. Additionally, chemotherapy-associated adverse events occurred more frequently with osimertinib plus chemotherapy than with placebo plus chemotherapy, likely due to a higher intracellular chemotherapy dose that is achieved in the presence osimertinib. However, formal studies are necessary to prove this. Moreover, the FLAURA2 clinical study, reported that combining osimertinib plus platinum-pemetrexed led to significantly longer overall survival compared with osimertinib monotherapy in first-line treatment in EGFR mutant NSCLC[39]. Further, the combination also demonstrated improved CNS efficacy[40]. The two trials discussed above (COMPEL and FLAURA2) may indicate that two drugs that compete for interaction with the same ABC transporter could enhance the efficacy of these anti-cancer drugs.

This work has been focused on ABCG2, but it seems reasonable to assume that our findings might also apply to other ABC transporters. Currently, there is a lack of systematic studies identifying which ABC transporters can export a given drug from cells. But since the vast majority of anti-cancer drugs are exported by at least one ABC transporter[41], it is possible that the mechanistic mode-of-action of many reported synergistic drug combinations are in fact ABC transporter-mediated. To explore this, future work should focus on creating a comprehensive drug-ABC transporter database, at least for clinically approved drugs and for drugs involved in reported synergistic drug combinations. Such a database will be invaluable to clarify the mechanisms underlying drug combination toxicity and for the identification of clinically safe drugs that could be repurposed as ABC inhibitors. This strategy may open new avenues for rational drug combination design, taking advantage of the overlooked role of ABC transporters in drug-drug synergistic interactions. Moreover, because ABC transporter variants are predictors of efficacy/toxicity of ABC transporter-dependent drugs[42], this knowledge would also help guide patient selection in clinical development.

# Methods

### Cell Culture and Reagents

The human non-small cell lung cancer (NSCLC) cell lines PC9 ($EGFR^{\Delta E746\text{-}A750}$), H1975 ($EGFR^{L858R/T790M}$) and H358 ($KRAS^{G12C}$) are part of the Bernards' Lab cell line collection. Cells were cultured in RPMI-1640 medium supplemented with 10% fetal bovine serum (FBS) and 1% penicillin/streptomycin at 37ºC in a 5% $CO_2$ atmosphere. Cell lines were authenticated by short-tandem-repeat DNA profiling. All cell lines were routinely tested for mycoplasma contamination (every 2 to 3 months). To generate gefitinib-resistant models (GRI and GRIII), parental PC9 cells were exposed to escalating concentrations of gefitinib (up to 2μM) for two months. Barasertib-resistant sublines (BaraRES) were generated by long-term (2-3 months) culture in escalating doses of barasertib.

### Compound Screening

To compose the stress-focused drug library, we considered the following stresses often associated with malignant phenotypes: DNA damage stress, oxidative stress, mitotic stress, proteotoxic stress, metabolic stress, and senescence/apoptosis evasion. Each compound was selected based on published data showing either induction of the respective stress or inhibition of the cellular responses to it. The range of doses was tailored according to published data about the compound, when available. On day 0, cells were plated in black-walled 384-well plates (Greiner #781091) at approximately 20% confluence. On the next day, the plates were divided into control (PC9) and drug-resistant (GRI and GRIII) arms. Gefitinib (2 μM) was added to the drug-resistant arms and then each library compound was added to both arms in 10 different doses (in triplicates) using the MICROLAB STAR liquid handling workstation (Hamilton). In each plate, phenylarsine oxide (10 μM) was used as positive control (0% cell viability) and DMSO was used as negative control (100% cell viability). After 5 days, resazurin (Sigma #R7017) was added to the plates. After 1 to 2 hours of incubation, fluorescence ($560_{Ex}/590_{Em}$) was recorded using the EnVision (PerkinElmer). The readings of each plate were then normalized using the positive and negative controls. The normalized values of each drug/dose were used to build dose-response viability curves. The AUC difference for each compound in the drug-resistant (GRI and GRIII) arms relative to control (PC9) was then calculated. All compounds were purchased from MedChemExpress.

For the large-scale drug repurposing screen, GRI cells were treated with the Oncode library (5,632 compounds) at a single concentration (1μM) alone or in combination with a sub-lethal dose (50 nM) of barasertib. The Oncode library is a repurposing library created by the Dutch Oncode institute (https://oncodeinstitute.nl/facilities/drug-repurposing-1). This library was created based on the previously published repurposing library of the Broad Institute[43] and contains compounds in different stages of human drug development.

**Cell Viability/Proliferation Assays**

Dose-response viability curves were performed in triplicate, using black-walled 384-well plates (Greiner #781091). Cells were plated with a 20% density (approximately) and incubated overnight for attachment. Drugs were then added to the cells using the Tecan D300e digital dispenser. 10 μmol/L phenylarsine oxide was used as positive control (0% cell viability) and DMSO was used as negative control (100% cell viability). Five days later, resazurin (Sigma #R7017) was added to the plates. After 1 to 4 hours of incubation (depending on the cell line), fluorescence ($560_{Ex}/590_{Em}$) was recorded using the EnVision (PerkinElmer). IC50 values were calculated using GraphPad Prism.

For colony formation assays, cells were plated at a low density in 12-well plates and incubated overnight for attachment. Drugs were then added to the cells using the Tecan D300e digital dispenser, as indicated. The culture media/drugs were refreshed every 2 to 3 days. When control wells were confluent, cells were fixed and stained for 20 to 30 minutes using a 1% formaldehyde (Millipore #104002)/1% methanol (Honeywell #32213)/0.05% crystal violet (Sigma #HT90132) solution in phosphate-buffered saline (PBS). Plates were then washed in water and left to dry before scanning.

Confluence assays were performed at least in triplicate, using black-walled 96-well plates (Greiner #655090). Cells were plated at a low density and incubated until attachment. Plates were then placed in the IncuCyte ZOOM (Essen Bioscience), which imaged the cells every 4 hours. Approximately 12 to 16 hours after plating, drugs were added to the cells using the Tecan D300e digital dispenser, as indicated. Phase-contrast images were collected and analyzed to detect cell proliferation based on confluence.

**Western Blotting**

After the indicated culture period and drug treatment, cells were washed with cold PBS, then lysed with RIPA buffer (25 mmol/L Tris-HCl, pH 7.6, 150 mmol/L NaCl, 1% NP-40, 1% sodium deoxycholate, 0.1% SDS) containing Complete Protease Inhibitor cocktail (Roche) and phosphatase inhibitor cocktails II and III (Sigma). Samples were then centrifuged for 15 minutes at 15,000 × g at 4°C and supernatant was collected. Protein concentration of the samples was normalized after performing a bicinchoninic acid (BCA) assay (Pierce BCA, Thermo Scientific), according to the manufacturer's instructions. Protein samples (denatured with DTT followed by 5 minutes of heating at 95°C) were then loaded in a 4% to 12% polyacrylamide gel. Gels were run (SDS-PAGE) for approximately 40 minutes at 180 volts. Proteins were transferred from the gel to a polyvinylidene fluoride (PVDF) membrane at 350 mA for 90 minutes. After the transfer, membranes were incubated in blocking solution (5% BSA in TBS with 0.1% Tween-20 (TBS-T). Subsequently, membranes were probed with the primary antibodies in 5% bovine serum albumin (BSA) overnight at 4°C. Membranes were then washed 3 times for 10 minutes with TBS-T, followed by 1-hour incubation at room temperature with the secondary antibody (HRP conjugated) in a blocking solution. Membranes were again washed 3 times for 5 minutes in TBS-T. Finally, a chemiluminescence substrate (ECL, Bio-Rad) was added to the membranes and the signal was imaged using the ChemiDoc-Touch (Bio-Rad).

The following antibodies were purchased from Cell Signaling Technology: EGFR #4267, Phospho-EGFR (Tyr1068) #3777, GAPDH #5174, Phospho-p44/42 MAPK (Erk1/2; Thr202/Tyr204) #4377, p44/42 MAPK (Erk1/2) #4695, Histone H3 #4499, Cleaved PARP (Asp214) #9546, ABCG2 #42078, AHR #83200. The antibodies α-Tubulin #T9026 and Vinculin #V9131 were purchased from Sigma-Aldrich. Phospho-Histone H3 (Ser10) #06-570 was purchased from MERCK (Upstate).

**Genomic Analysis and RNA Sequencing**

Genomic DNA was isolated using Quick-DNA Miniprep (Zymo Research # D3025) and *EGFR* exon 20 was amplified by PCR (FW primer: ATCGCATTCATGCGTCTTCAC. RV primer: ACACATATCCCCATGGCAAACT) and analyzed by Sanger sequencing to detect the T790M mutation.

For transcriptomic analysis, RNA was extracted from untreated cells and cells treated with gefitinib (2 μM), barasertib (100 nM), or the combination for 24 hours. For harvesting, the cells were scraped into 15 mL tubes, washed once with cold PBS, and homogenized in RLT buffer (Qiagen #79216). Total RNA was isolated using the RNeasy Mini Kit (74106, Qiagen) including an on-column DNase digestion (79254, Qiagen), according to the manufacturer's instructions. Quality and quantity of the total RNA were

assessed on the 2100 Bioanalyzer instrument following the manufacturer's instructions "Agilent RNA 6000 Nano" (G2938-90034, Agilent Technologies). Total RNA samples were subjected to TruSeq stranded mRNA library preparation, according to the manufacturer's instructions (Document #1000000040498 v00, Illumina). The stranded mRNA libraries were analyzed on a 2100 Bioanalyzer instrument following the manufacturer's protocol "Agilent DNA 7500 kit" (G2938-90024, Agilent Technologies), diluted to 10 nmol/L and pooled equimolar into multiplex sequencing pools for paired-end sequencing on the NovaSeq 6000 Illumina sequencing instrument. Paired-end sequencing was performed using 54 cycles for Read 1, 19 cycles for Read i7, 10 cycles for Read i5, and 54 cycles for Read 2, using the NovaSeq6000 SP Reagent Kit v1.5 (100 cycles; 20028401, Illumina). For the analysis, the RNA-seq count data were normalized using a relative total size factor. The data set was then filtered for protein-coding genes. Log2 fold change and mean values were calculated for each treatment compared with untreated. The data were filtered for low counts using a filter of mean greater or equal to 10 in order to obtain robust scores. A Gene Set Enrichment Analysis (GSEA) was performed using the Hallmarks gene set collection using the R-package fGSEA (BioRxiv, 2021.10.1101/060012), which calculates a NES score and a P value.

**CRISPR/Cas9 Screens and Genetic Engineering**

A genome-wide CRISPR knockout screen was performed in GRI cells expressing Cas9 (lentiCas9-Blast, Addgene #52962) using the Brunello sgRNA library (Addgene #73178). The appropriate number of cells to achieve a 250-fold representation of the Brunello library for all the screen arms and replicates were transduced at approximately 50% confluence in the presence of polybrene (8 µg/mL) with the appropriate volume of the lentiviral-packaged sgRNA library. Cells were incubated overnight, followed by the replacement of the lentivirus-containing medium with fresh medium containing puromycin (2 µg/mL). The lentivirus volume to achieve a multiplicity of infection (MOI) of 0.3, as well as the puromycin concentration to achieve a complete selection in 3 days, was previously determined. After puromycin selection, cells were split into the indicated arms/replicates (for each arm, the appropriate number of cells to keep a 250-fold representation of the library was plated at approximately 10%–20% confluence) and a T0 (reference) time point was harvested. Cells were maintained as indicated and, in case a passage was required, cells were reseeded at the appropriate number to keep at least a 250-fold representation of the library. Cells were harvested after about 8 population doublings, washed with PBS, pelleted, and stored at −80°C until DNA extraction.

Genomic DNA was extracted (Zymo Research, D3024) from cell pellets according to the manufacturer's instructions. For every sample, DNA was quantified and the necessary DNA to maintain a 250-fold representation of the library was used for subsequent procedures (for this, we assumed that each cell contains 6.6 pg genomic DNA). Each sample was divided over 50 µL PCR reactions (using a maximum of 1 µg genomic DNA per reaction) using barcoded forward primers to be able to deconvolute multiplexed samples after next-generation sequencing. PCR mixture per reaction: 10 µL 5× HF Buffer, 1 µL 10 µmol/L forward primer, 1 µL 10 µmol/L reverse primer, 0.5 µL Phusion polymerase (Thermo Fisher, F-530XL), 1 µL 10 mmol/L dNTPs, adding $H_2O$ and template to 50 µL. Cycling conditions: 30 seconds at

98°C, 20× (30 seconds at 98°C, 30 seconds at 60°C, 1 minutes at 72°C), 5 minutes at 72°C. The products of all reactions from the same sample were pooled, and 2 µL of this pool was used in a subsequent PCR reaction using primers containing adapters for next-generation sequencing. The same cycling protocol was used, however this time for 15 cycles. Next, PCR products were purified using the Bioline ISOLATE II PCR and Gel Kit (GC Biotech, BIO-52060) according to the manufacturer's instructions. DNA concentrations were measured and, based on this, samples were pooled equimolarly.

The pool of amplified sgRNA sequences was sequenced on an Illumina HiSeq 2500 with a high-output kit (Single-Read, 65 bp). The reads were mapped to the unique barcodes used for each sample and sgRNA sequences of the Brunello library. Mapped read counts were normalized for sequencing depth as follows: for each sample, a size factor was calculated by taking the total count for that sample and dividing it by the geometric mean of the total counts across all samples. All counts within each sample were then divided by the corresponding size factor. A pseudo-count of 1 was added to all count values to prevent undefined log2 fold changes in later calculations. A differential analysis at the sgRNA level was performed using DESeq2[44]. The results from DESeq2 were used as input for gene-level enrichment analysis using MAGeCK's RRA algorithm[45], resulting in an FDR value. The gene-level log2 fold change was calculated as the median of the log2 fold changes of the sgRNAs targeting that gene, as obtained from the sgRNA-level differential analysis.

For validation, individual KOs were generated. The top sgRNAs from the CRISPR screen were cloned into lentiGuide-Puro (Addgene #52963). ABCG2 overexpression was achieved using CRISPR-activation technology (lenti dCAS-VP64_Blast and pXPR_502, Addgene #61425 and #96923).

EGFR knockdown was performed using lentiviral shRNA (pLKO.1 system). TRCN0000039633: GCTGAGAATGTGGAATACCTA.

### *In Vivo* PDX Models

Primary tumors were obtained from Bellvitge Hospital (HUB) and the Catalan Institute of Oncology (ICO) with approval from the Ethical Committee (CEIC Bellvitge Hospital), ethical and legal protection guidelines for human subjects, including written informed consent, in accordance with the Declaration of Helsinki. The experimental design was approved by the IDIBELL animal facility committee. All animal experiments were performed following the guidelines for Ethical Conduct in the Care and Use of Animals as stated in the International Guiding Principles for Bio-medical Research Involving Animals, developed by the Council for International Organizations of Medical Sciences.

PDX1 was generated from a lung adenocarcinoma biopsy from a patient who was treated with Erlotinib (first line), Gefitinib + Capmatinib (second line) and Carboplatin+Gemcitabine and Nivolumab (third line). This tumour has an EGFR mutation (L858R) and MET amplification. PDX2 was generated from a lung adenocarcinoma biopsy from a patient who was treated with Afatinib (first line) and CBDCA + pemetrexed (second line). This tumour has a germline p53 mutation and EGFR mutation (del19).

Briefly, to establish the PDX models, a small tumor piece of 2 to 4 $mm^3$ maintaining tridimensional structure was anchored with Prolene 7.0 to the serosa of the caecum of two 5- to 6-week-old male athymic nude mice (strain Hsd:Athymic Nude-Foxn1nu) purchased from Envigo. After implantation, mice were inspected twice a week. At euthanasia, the tumors were harvested, cut into small fragments, and serially transplanted into new animals for tumor perpetuation or experimental treatment procedures.

Tumors were implanted subcutaneously into Crl:NU-Foxn1nu mice. Tumor volume and mouse body weight were monitored twice weekly. When tumors reached a volume of approximately 200–600 mm3, mice were randomized into four groups: vehicle, gefitinib (60 mg/kg), barasertib (50 mg/kg), or the combination. Drugs were formulated in DMSO: Kolliphor EL (Sigma 27963): Saline solution, in a ratio of (1:1:8). Mice were treated 5 days a week (Monday to Friday) at the indicated doses by intraperitoneal injection.

### Statistics and Reproducibility

With the exceptions of CRISPR screens, drug screens and RNA-seq, each *in vitro* experiment has been independently reproduced with similar results. GraphPad Prism 10 was used for the statistical analyses. Data are presented as mean ± SEM from at least three independent experiments. ZIP synergy scores were calculated using the SynergyFinder web tool.

### Reporting summary

Further information on research design is available in the Nature Portfolio Reporting Summary linked to this article.

## Declarations

### Data availability

The data from the CRISPR and compound screens are provided in Supplementary Tables. The raw data can be provided upon request from the corresponding authors. All other data generated or analyzed during the study are available upon request from the corresponding authors.

### Acknowledgments

We thank the members of the Bernards laboratory for helpful discussion and thoughtful feedback. We thank the genomics core facility of the Netherlands Cancer Institute (NKI).

This work was supported by an institutional grant of the Dutch Cancer Society and of the Dutch Ministry of Health, Welfare and Sport and by the Oncode Institute.

This research was funded by the Instituto de Salud Carlos III [co-funded by the European Regional Development Fund - Fondo Europeo de Desarrollo Regional (FEDER), "a way to build Europe/una manera

de hacer Europa"] through the grant PI22/00548 (to A.Villanueva) and by the Health and Science Departments of the Catalan Government (Generalitat de Catalunya) (2021SGR00184 to A.Villanueva)

**Author contributions**

J.M.F.N., M.H.D. and R.B. conceived and designed the research. J.M.F.N., C.P., N.P., B.M., E.N., E.F., L.F., J.F.M.T., A.V. and M.H.D. performed experimental work and curated data. J.M.F.N., C.P., N.P., C.L. and M.H.D. analyzed data and prepared figures. J.M.F.N., E.N., A.V., R.L.B, M.H.D. and R.B. supervised the research. A.V. and R.B. acquired funding for this research. J.M.F.N., M.H.D. and R.B. wrote the manuscript. All authors interpreted data and edited the manuscript.

**Competing interests**

Alberto Villanueva and August Vidal:

- co-founders and shareholders of Xenopat S.L. (Barcelona, Spain).

Ernest Nadal:

- Research funding: Roche, Pfizer, Merck-Serono, Bristol Myers Squibb and Boehringer-Ingelheim.
- Advisory board or lectures: Amgen, Apollomics, AstraZeneca, BeiGene, BMS, Boehringer-Ingelheim, Daiichi-Sankyo, Genmab, Glaxo Smith Kline, Illumina, Johnson & Johnson, Lilly, Merck Sharp & Dohme (MSD), Merck-Serono, Pfizer, PharmaMar, Pierre Fabre, Qiagen, Regeneron, Roche, Sanofi, Summit Therapeutics and Takeda.
- Travel support: Roche, Takeda, Janssen and MSD.

# References

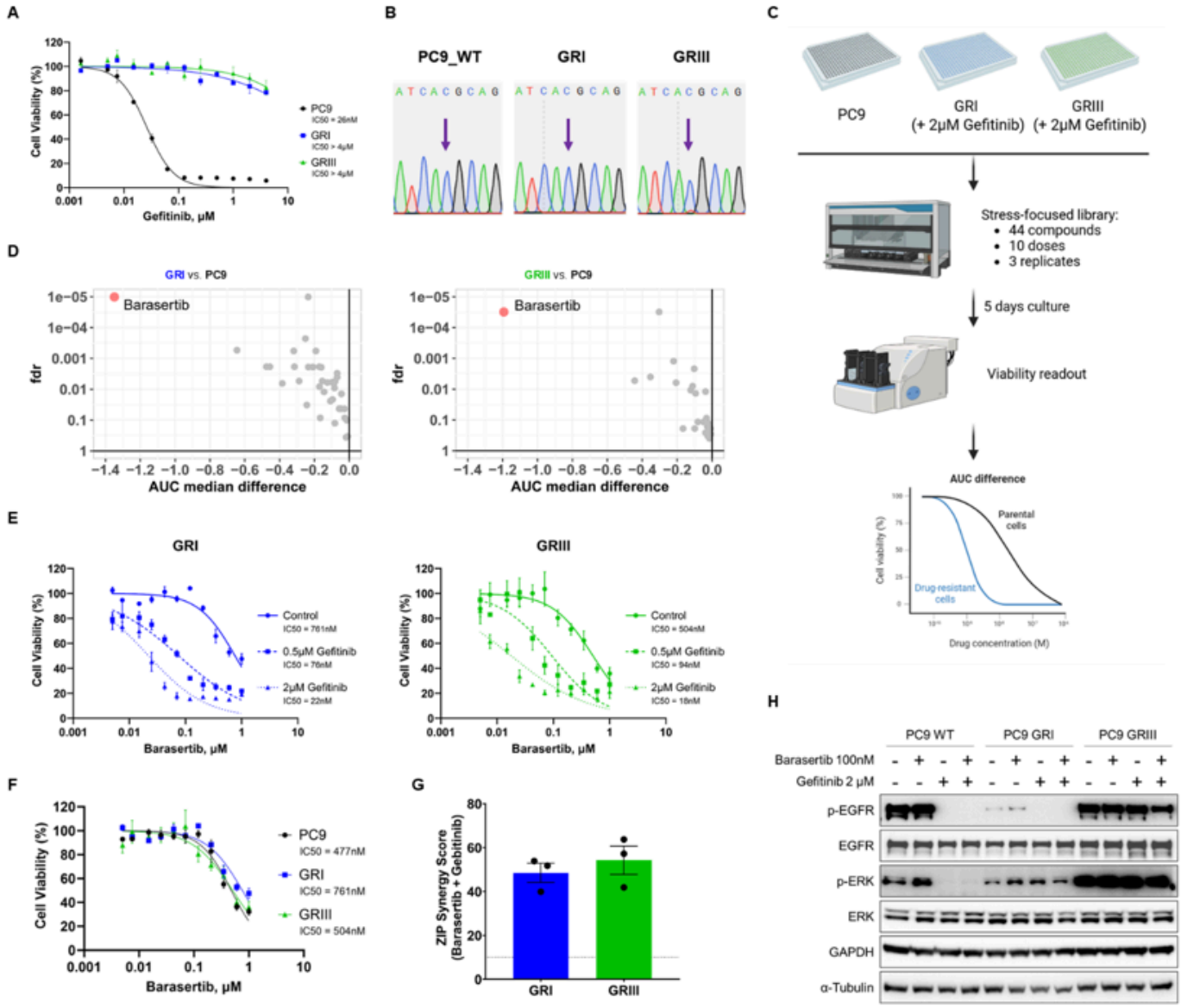
1. Bray, F. *et al.* Global cancer statistics 2022: GLOBOCAN estimates of incidence and mortality worldwide for 36 cancers in 185 countries. *CA. Cancer J. Clin.* **74**, 229–263 (2024).
2. Ashrafi, A. *et al.* Current Landscape of Therapeutic Resistance in Lung Cancer and Promising Strategies to Overcome Resistance. *Cancers* **14**, 4562 (2022).
3. Smolarz, B. *et al.* Lung Cancer—Epidemiology, Pathogenesis, Treatment and Molecular Aspect (Review of Literature). *Int. J. Mol. Sci.* **26**, 2049 (2025).
4. Skoulidis, F. & Heymach, J. V. Co-occurring genomic alterations in non-small-cell lung cancer biology and therapy. *Nat. Rev. Cancer* **19**, 495–509 (2019).
5. Ricordel, C., Friboulet, L., Facchinetti, F. & Soria, J.-C. Molecular mechanisms of acquired resistance to third-generation EGFR-TKIs in EGFR T790M-mutant lung cancer. *Ann. Oncol.* **29**, i28–i37 (2018).
6. Zhou, X. *et al.* Strategies Beyond 3rd EGFR-TKI Acquired Resistance: Opportunities and Challenges. *Cancer Med.* **14**, e70921 (2025).

7. Hendriks, L. E. *et al.* ESMO Oncogene-Addicted Non-Small Cell Lung Cancer Living Guideline v1.3. https://www.esmo.org/guidelines/living-guidelines/esmo-living-guideline-oncogene-addicted-metastatic-non-small-cell-lung-cancer (2026).
8. Hendriks, L. E. *et al.* Oncogene-addicted metastatic non-small-cell lung cancer: ESMO Clinical Practice Guideline for diagnosis, treatment and follow-up. *Ann. Oncol.* **34**, 339–357 (2023).
9. Cooper, A. J., Sequist, L. V. & Lin, J. J. Third-generation EGFR and ALK inhibitors: mechanisms of resistance and management. *Nat. Rev. Clin. Oncol.* **19**, 499–514 (2022).
10. Tanaka, K. *et al.* Targeting Aurora B kinase prevents and overcomes resistance to EGFR inhibitors in lung cancer by enhancing BIM- and PUMA-mediated apoptosis. *Cancer Cell* **39**, 1245-1261.e6 (2021).
11. Shah, K. N. *et al.* Aurora kinase A drives the evolution of resistance to third-generation EGFR inhibitors in lung cancer. *Nat. Med.* **25**, 111–118 (2019).
12. Park, M.-Y. *et al.* Generation of lung cancer cell lines harboring EGFR T790M mutation by CRISPR/Cas9-mediated genome editing. *Oncotarget* **8**, 36331–36338 (2017).
13. Luo, J., Solimini, N. L. & Elledge, S. J. Principles of cancer therapy: oncogene and non-oncogene addiction. *Cell* **136**, 823–837 (2009).
14. Yadav, B., Wennerberg, K., Aittokallio, T. & Tang, J. Searching for Drug Synergy in Complex Dose-Response Landscapes Using an Interaction Potency Model. *Comput. Struct. Biotechnol. J.* **13**, 504–513 (2015).
15. Marchetti, S. *et al.* Effect of the drug transporters ABCG2, Abcg2, ABCB1 and ABCC2 on the disposition, brain accumulation and myelotoxicity of the aurora kinase B inhibitor barasertib and its more active form barasertib-hydroxy-QPA. *Invest. New Drugs* **31**, 1125–1135 (2013).
16. Taylor, N. M. I. *et al.* Structure of the human multidrug transporter ABCG2. *Nature* **546**, 504–509 (2017).
17. Cusatis, G. *et al.* Pharmacogenetics of ABCG2 and adverse reactions to gefitinib. *J. Natl. Cancer Inst.* **98**, 1739–1742 (2006).
18. Galetti, M. *et al.* Effect of ABCG2/BCRP Expression on Efflux and Uptake of Gefitinib in NSCLC Cell Lines. *PLOS ONE* **10**, e0141795 (2015).
19. Lemos, C. *et al.* Impact of ABCG2 Polymorphisms on the Clinical Outcome and Toxicity of Gefitinib in Non-Small-Cell Lung Cancer Patients. *Pharmacogenomics* **12**, 159–170 (2011).
20. Yanase, K. *et al.* Gefitinib reverses breast cancer resistance protein–mediated drug resistance. *Mol. Cancer Ther.* **3**, 1119–1125 (2004).
21. Burger, H. *et al.* Imatinib mesylate (STI571) is a substrate for the breast cancer resistance protein (BCRP)/ABCG2 drug pump. *Blood* **104**, 2940–2942 (2004).
22. Baek, S. H. When Signaling Kinases Meet Histones and Histone Modifiers in the Nucleus. *Mol. Cell* **42**, 274–284 (2011).

23. Hirota, T., Lipp, J. J., Toh, B.-H. & Peters, J.-M. Histone H3 serine 10 phosphorylation by Aurora B causes HP1 dissociation from heterochromatin. *Nature* **438**, 1176–1180 (2005).
24. Drug Repurposing Programme | Oncode Institute. https://www.oncodeinstitute.nl/drug-repurposing-programme.
25. Balabanov, S. *et al.* Abcg2 overexpression represents a novel mechanism for acquired resistance to the multi-kinase inhibitor Danusertib in BCR-ABL-positive cells in vitro. *PloS One* **6**, e19164 (2011).
26. Kathawala, R. J. *et al.* ABCG2 Overexpression Contributes to Pevonedistat Resistance. *Cancers* **12**, 429 (2020).
27. Sun, D., Gao, W., Hu, H. & Zhou, S. Why 90% of clinical drug development fails and how to improve it? *Acta Pharm. Sin. B* **12**, 3049–3062 (2022).
28. Hutchinson, L. & Kirk, R. High drug attrition rates—where are we going wrong? *Nat. Rev. Clin. Oncol.* **8**, 189–190 (2011).
29. Jentzsch, V., Osipenko, L., Scannell, J. W. & Hickman, J. A. Costs and Causes of Oncology Drug Attrition With the Example of Insulin-Like Growth Factor-1 Receptor Inhibitors. *JAMA Netw. Open* **6**, e2324977 (2023).
30. Löwenberg, B. *et al.* Phase 1/2 study to assess the safety, efficacy, and pharmacokinetics of barasertib (AZD1152) in patients with advanced acute myeloid leukemia. *Blood* **118**, 6030–6036 (2011).
31. Kantarjian, H. M. *et al.* Stage I of Phase II study assessing efficacy, safety and tolerability of barasertib (AZD1152) versus LDAC in elderly AML patients. *Cancer* **119**, 2611–2619 (2013).
32. Piccoli, L. *et al.* Role of Orexin-1 Receptor Mechanisms on Compulsive Food Consumption in a Model of Binge Eating in Female Rats. *Neuropsychopharmacology* **37**, 1999–2011 (2012).
33. van Hoppe, S. *et al.* Brain accumulation of osimertinib and its active metabolite AZ5104 is restricted by ABCB1 (P-glycoprotein) and ABCG2 (breast cancer resistance protein). *Pharmacol. Res.* **146**, 104297 (2019).
34. Fan, Y. *et al.* Lazertinib improves the efficacy of chemotherapeutic drugs in ABCB1 or ABCG2 overexpression cancer cells in vitro, in vivo, and ex vivo. *Mol. Ther. - Oncolytics* **24**, 636–649 (2022).
35. BCRP/ABCG2 Inhibitors | DrugBank. https://go.drugbank.com/categories/DBCAT002662.
36. BCRP/ABCG2 Substrates | DrugBank. https://go.drugbank.com/categories/DBCAT002663.
37. Peled, N. *et al.* COMPEL: osimertinib plus platinum-based chemotherapy in patients with EGFR-mutated advanced NSCLC and progression on first-line osimertinib. *ESMO Open* **10**, (2025).
38. Li, L., Sham, Y. Y., Bikadi, Z. & Elmquist, W. F. pH-Dependent Transport of Pemetrexed by Breast Cancer Resistance Protein. *Drug Metab. Dispos.* **39**, 1478–1485 (2011).
39. Jänne, P. A. *et al.* Survival with Osimertinib plus Chemotherapy in EGFR-Mutated Advanced NSCLC. *N. Engl. J. Med.* **394**, 27–38 (2025).
40. Jänne, P. A. *et al.* CNS Efficacy of Osimertinib With or Without Chemotherapy in Epidermal Growth Factor Receptor–Mutated Advanced Non–Small-Cell Lung Cancer. *J. Clin. Oncol.* **42**, 808–820

(2024).
41. DrugBank - PubChem Data Source. https://pubchem.ncbi.nlm.nih.gov/source/DrugBank.
42. Morau, M. V., Seguin, C. S., Visacri, M. B., Pincinato, E. de C. & Moriel, P. Genetic Variants in the ABCB1 and ABCG2 Gene Drug Transporters Involved in Gefitinib-Associated Adverse Reaction: A Systematic Review and Meta-Analysis. *Genes* **15**, 591 (2024).
43. Corsello, S. M. *et al.* The Drug Repurposing Hub: a next-generation drug library and information resource. *Nat. Med.* **23**, 405–408 (2017).
44. Love, M. I., Huber, W. & Anders, S. Moderated estimation of fold change and dispersion for RNA-seq data with DESeq2. *Genome Biol.* **15**, 550 (2014).
45. Li, W. *et al.* MAGeCK enables robust identification of essential genes from genome-scale CRISPR/Cas9 knockout screens. *Genome Biol.* **15**, 554–554 (2014).

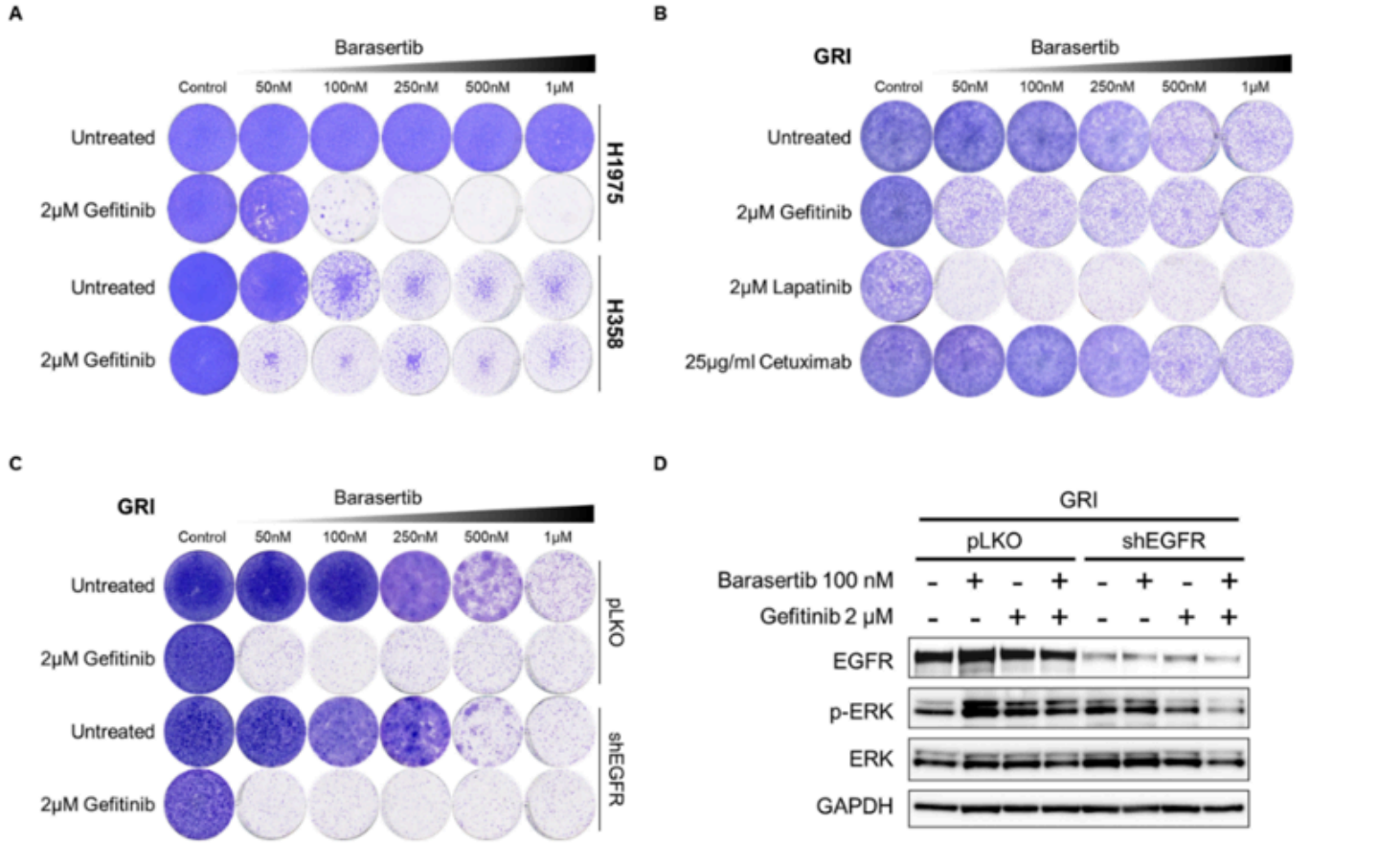
# Figures




## Figure 1

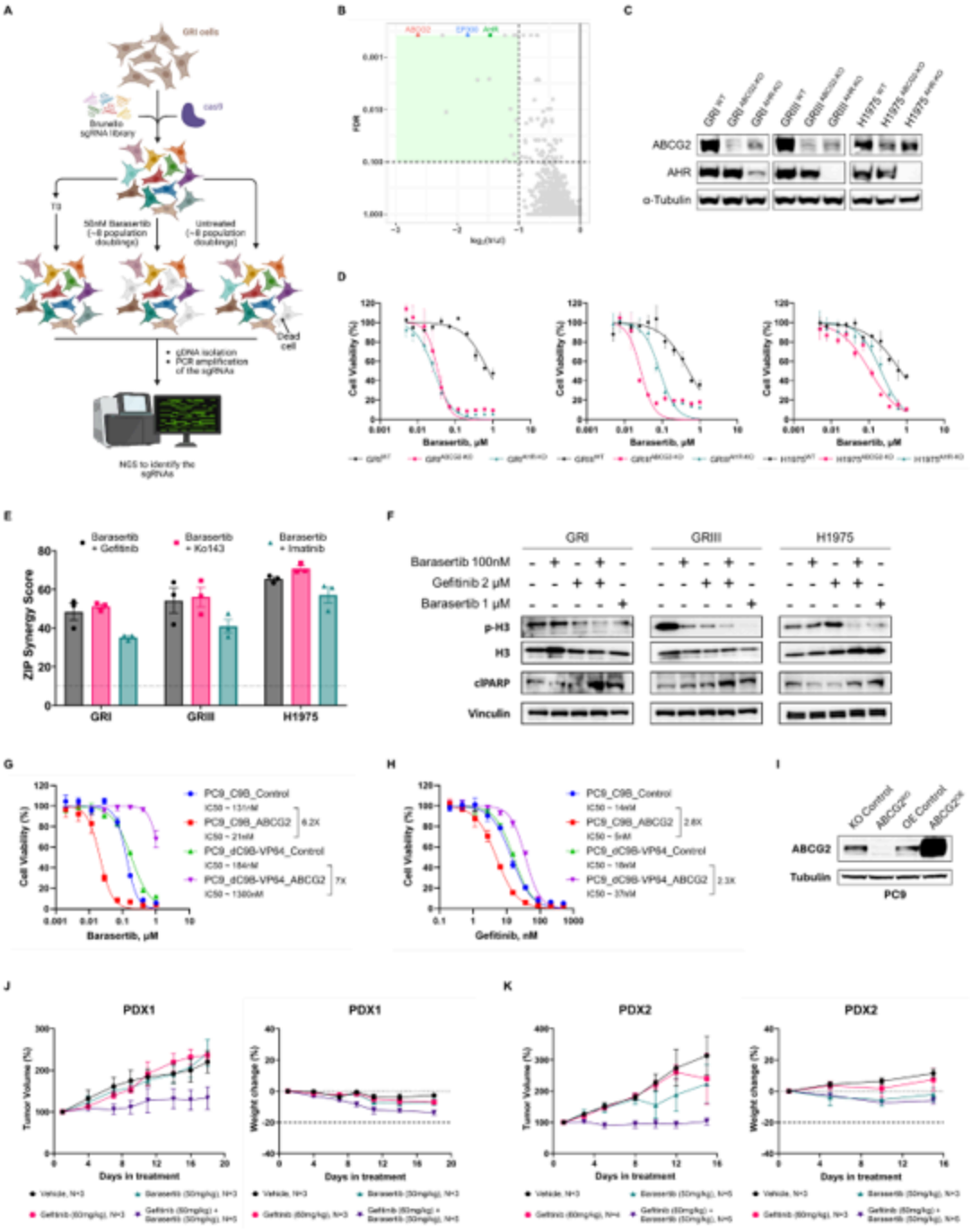
**Gefitinib enhances the sensitivity of Gefitinib-resistant PC9 cells to Barasertib.**
(A) Dose-response viability curves of parental PC9 (black), GRI (blue), and GRIII (green) cells treated with increasing concentrations of gefitinib for 5 days. Data represent mean ± SEM (n = 3). IC50 values are indicated. (B) Sanger sequencing chromatograms of EGFR exon 20 in parental PC9, GRI, and GRIII cells. The arrow indicates the C>T substitution (T790M) present in GRIII but absent in GRI. (C) Schematic of the stress-focused compound screen. GRI and GRIII cells were screened against 44 compounds in the presence of 2μM gefitinib. Viability was assessed after 5 days. (D) Volcano plots showing the results of the compound screen for GRI vs. PC9 (left) and GRIII vs. PC9 (right). The x-axis represents the median difference in Area Under the Curve (AUC). The y-axis represents the false discovery rate (FDR). Barasertib (red) is identified as the top hit in both resistant lines. (E) Dose-response viability curves of GRI (left) and GRIII (right) cells treated with increasing concentrations of barasertib, alone or in combination with 0.5μM or 2μM gefitinib, for 5 days. Data represent mean ± SEM (n = 3). (F) Dose-response viability curves

comparing parental PC9, GRI, and GRIII cells treated with increasing concentrations of barasertib for 5 days. Data represent mean ± SEM (n = 3). (G) Zero Interaction Potency (ZIP) synergy scores for the combination of barasertib and gefitinib in GRI and GRIII cells. Scores >10 indicate significant synergy. Data represent mean ± SEM (n = 3). (H) Western blot analysis of EGFR signaling in PC9 WT, GRI, and GRIII cells treated with barasertib (100 nM), gefitinib (2 μM), or the combination for 24 hours. GAPDH and α-Tubulin were used as loading controls.




## Figure 2

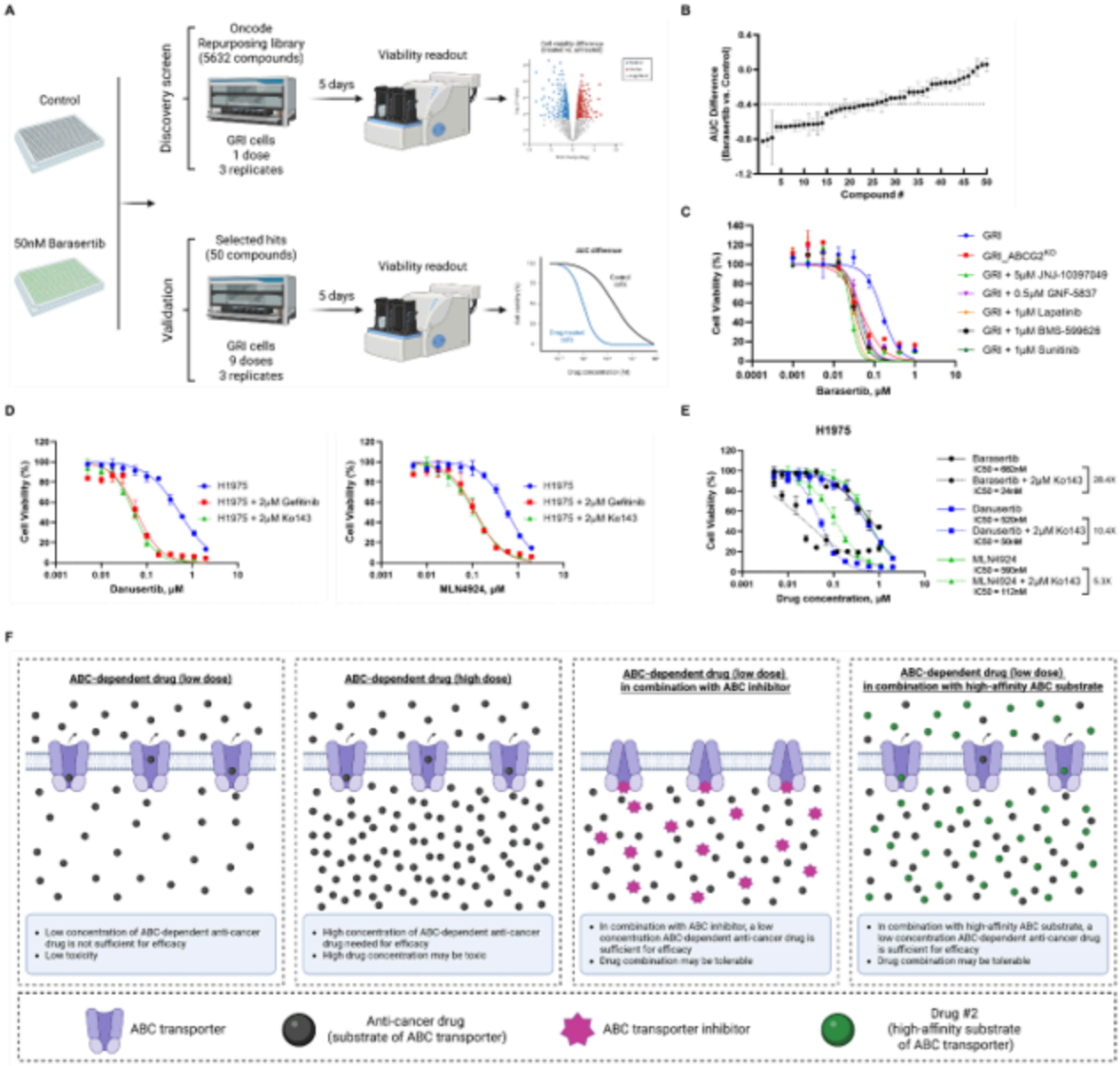
**The synergy between EGFR inhibitor Gefitinib and Barasertib is independent of EGFR inhibition.**
(A) Colony formation assays of H1975 ($EGFR^{L858R/T790M}$) and H358 ($KRAS^{G12C}$) cells treated with increasing concentrations of barasertib alone or in combination with 2μM gefitinib for 10 days. (B) Colony formation assays of GRI cells treated with increasing concentrations of barasertib in combination with different EGFR inhibitors: gefitinib (2μM), lapatinib (2μM), or cetuximab (25μg/mL). (C) Colony formation assays of GRI cells following lentiviral transduction with a non-targeting control (pLKO) or an shRNA targeting EGFR (shEGFR), treated with barasertib and gefitinib as indicated. (D) Western blot analysis confirming EGFR knockdown and downstream ERK phosphorylation in GRI cells expressing pLKO or shEGFR, treated with barasertib (100 nM), gefitinib (2μM), or the combination for 24 hours. GAPDH was used as a loading control.




## Figure 3

**Gefitinib sensitizes NSCLC cells to Barasertib by reducing ABCG2-mediated barasertib efflux.**
(A) Schematic representation of the genome-wide CRISPR/Cas9 knockout screen in GRI cells treated with a non-lethal dose of barasertib (50 nM) to identify sensitizing hits. (B) Volcano plot displaying depleted sgRNAs in barasertib-treated GRI cells. Significant hits including ABCG2 (red) and its transcriptional regulators EP300 (blue) and AHR (green) are highlighted. (C) Western blot validation of ABCG2 and AHR knockout (KO) in GRI, GRIII, and H1975 cell lines. A-Tubulin was used as a loading control. (D) Dose-response viability curves of GRI, GRIII and H1975 cells, comparing wild-type (WT) to

ABCG2-KO and AHR-KO subclones treated with increasing concentrations of barasertib. € ZIP synergy scores in GRI, GRIII, and H1975 cells for barasertib in combination with gefitinib, Ko143 or imatinib. Data represent mean ± SEM (n = 3). (F) Western blot analysis of hosphor-Histone H3 (p-H3), total H3, and cleaved PARP (clPARP) in GRI, GRIII, and H1975 cells treated with barasertib (100 nM), gefitinib (2μM), the combination, or a high dose of barasertib (1μM) for 24 hours. Vinculin was used as a loading control. (G, H) Dose-response viability curves of PC9 cells with CRISPR-mediated knockout (C9B) or CRISPR-activation (dC9B-VP64) of ABCG2 treated with increasing concentrations of barasertib (G) or gefitinib (H) for 5 days. Fold-change in sensitivity is indicated. (I) Western blot confirming ABCG2 knockout and overexpression in PC9 cells. A-Tubulin was used as a loading control. (J, K) *In vivo* efficacy of vehicle, gefitinib (60 mg/kg), barasertib (50 mg/kg), or the combination in two EGFR-inhibitor resistant patient-derived xenograft (PDX) models: PDX1 (K) and PDX2 (L). Left: Tumor volume over time; Right: Mouse body weight change. Data represent mean ± SEM.




## Figure 4

**Drugs with ABC transporter activity increase the efficacy of targeted anti-cancer drugs.**
(A) Schematic representation of the workflow of the high-throughput discovery screen and subsequent validation. GRI cells were screened against 5,632 compounds (Oncode Repurposing library) at a single dose ± 50 nM barasertib. 50 hits were selected for 9-dose validation to determine the change in Area Under the Curve (AUC). (B) Rank-ordered plot of 50 validated hits based on the AUC difference (barasertib vs. control). Compounds below the dashed line (<-0.4) show significant sensitization to barasertib. (C) Dose-response viability curves of GRI cells treated with increasing concentrations of barasertib for 5 days, in the absence or presence of various screen hits: JNJ-10397049 (5μM), GNF-5837 (0.5μM), lapatinib (1 μM), BMS-599626 (1μM), and sunitinib (1μM). ABCG2 KO cells were used as

positive control for expected sensitization by ABCG2 activity. (D) Dose-response viability curves of H1975 cells treated with increasing concentrations of danusertib (left) or MLN4924 (right) for 5 days, alone or in combination with gefitinib (2μM) or Ko143 (2μM). € Comparison of the sensitizing effect of Ko143 (2μM) on barasertib, danusertib, and MLN4924 in H1975 cells. Fold-reduction in IC50 is indicated for each drug. Data represent mean ± SEM (n = 3). (F) Proposed model for ABCG2-mediated synergistic interactions. Left: Low doses of ABC-dependent drugs are quickly effluxed, leading to insufficient intracellular drug concentration to achieve efficacy. Middle-Left: High doses achieve efficacy but may cause toxicity. Right panels: Combining an ABC-dependent drug at low dose with either an ABC inhibitor (e.g., Ko143) or a high-affinity substrate (e.g., gefitinib) decreases the efflux rate, thereby maintaining sufficient intracellular drug concentration to achieve efficacy, possibly at tolerable doses.

## Supplementary Files

This is a list of supplementary files associated with this preprint. Click to download.

- Table1StressfocusedMinilibrary.xlsx
- Table2ResultsStressfocusedLibraryScreen.xlsx
- Table3ResultsBrunelloCRISPRScreen.xlsx
- Table4ResultsRepurposingScreen.xlsx
- Table5ResultsRepurposingScreenValidation.xlsx